
Neural Signed Distance Function Inference through Splatting 3D Gaussians Pulled on Zero-Level Set

Wenyuan Zhang¹, Yu-Shen Liu^{1*}, Zhizhong Han²

School of Software, Tsinghua University, Beijing, China¹

zhangwen21@mails.tsinghua.edu.cn, liuyushen@tsinghua.edu.cn

Department of Computer Science, Wayne State University, Detroit, USA²

h312h@wayne.edu

Abstract

It is vital to infer a signed distance function (SDF) in multi-view based surface reconstruction. 3D Gaussian splatting (3DGS) provides a novel perspective for volume rendering, and shows advantages in rendering efficiency and quality. Although 3DGS provides a promising neural rendering option, it is still hard to infer SDFs for surface reconstruction with 3DGS due to the discreteness, the sparseness, and the off-surface drift of 3D Gaussians. To resolve these issues, we propose a method that seamlessly merge 3DGS with the learning of neural SDFs. Our key idea is to more effectively constrain the SDF inference with the multi-view consistency. To this end, we dynamically align 3D Gaussians on the zero-level set of the neural SDF using neural pulling, and then render the aligned 3D Gaussians through the differentiable rasterization. Meanwhile, we update the neural SDF by pulling neighboring space to the pulled 3D Gaussians, which progressively refine the signed distance field near the surface. With both differentiable pulling and splatting, we jointly optimize 3D Gaussians and the neural SDF with both RGB and geometry constraints, which recovers more accurate, smooth, and complete surfaces with more geometry details. Our numerical and visual comparisons show our superiority over the state-of-the-art results on the widely used benchmarks. Project page: <https://wen-yuan-zhang.github.io/GS-Pull>.

1 Introduction

3D scene representations are important to various computer vision applications, such as single or multi-view 3D reconstruction [39, 42, 67, 72], novel view synthesis [1, 71], and neural SLAM [22, 32, 78, 24] etc.. Mesh and point clouds are the most common 3D scene representations, and can be rendered by fast rasterization on GPUs. Instead, more recent neural radiance fields (NeRFs) [49] are continuous scene representations, but it is slow to render NeRFs due to the need of costly stochastic sampling along rays in volume rendering. More recently, 3D Gaussians with different attributes like color and opacity are used as a versatile differentiable volumetric representation [30, 77, 23] for neural rendering through splatting, dubbed 3D Gaussian Splatting (3DGS). It prompts the pros of both NeRFs and point based representations, which achieves both better quality and faster speed in rendering. Although 3D Gaussians can render plausible images, it is still a challenge to reconstruct surfaces based on the 3D Gaussians.

The key challenge comes from the gap between the discrete 3D Gaussians and the continuous geometry representations, such as implicit functions. Besides the discreteness, the sparseness caused by uneven distribution and the off-surface drift make 3D Gaussians even harder to use than

*The corresponding author is Yu-Shen Liu.

scanned point clouds in surface inference. To overcome these obstacles, recent solutions usually add previous volume rendering based reconstruction methods [60, 50] to 3DGS as a complement branch [44, 66, 11], use monocular depth and normal images as priors to bypass the messy and unordered 3D Gaussians [14, 57], or use surface-aligned Gaussians [25, 68, 14] in rasterization to approximate surfaces. However, how to learn continuous implicit representations to recover more accurate, smooth, and complete surfaces with sharp geometry details is still an open question.

To answer this question, we introduce a novel method to infer neural SDFs from multi-view RGB images through 3D Gaussian splatting. We progressively infer a signed distance field by training a neural network along with learning 3D Gaussians to minimize rendering errors through splatting. To more effectively constrain the surface inference with the multi-view consistency, we dynamically align 3D Gaussians with the zero-level set of the neural SDF, and render the aligned 3D Gaussians on the zero-level set by differentiable rasterization. Meanwhile, we update the neural SDF by pulling the neighboring space onto the disk determined by each 3D Gaussian on the zero-level set, which gradually refines the signed distance field near the surface. The capability of seamlessly merging neural SDFs with 3DGS not only get rid of the dependence of costly NeRFs like stochastic sampling on rays but also enables us to access the field attributes like signed distances and gradients during the splatting process, which provides a novel perspective and a versatile platform for surface reconstruction with 3DGS. The key to the 3D Gaussian alignment and neural SDF inference is a differentiable pulling operation which uses the predicted signed distances and gradients from the neural SDF. It provides a way of imposing geometry based constraints on 3D Gaussians besides the RGB based constraints through splatting. Our numerical and visual evaluations on widely used benchmarks show our superiority over the latest methods in terms of reconstruction accuracy and recovered geometry details. Our contributions are listed below,

- We propose to infer neural SDF through splatting 3D Gaussians pulled on the zero-level set, which can more effectively constrain surface inference with the multi-view consistency. This enables to recover more accurate, smooth, and complete surfaces with geometry details.
- We introduce to dynamically align 3D Gaussians to the zero-level set and update the neural SDF through a differentiable pulling operation. To this end, we propose novel loss terms and training strategies to work with the discrete and sparse 3D Gaussians in surface reconstruction.
- We achieve the state-of-the-art numerical and visual results in multi-view based surface reconstruction.

2 Related Work

Neural implicit representations have achieved remarkable progress in reconstructing 3D geometry with details [53, 48, 13, 45, 7, 21]. Neural implicit functions can be learned by either 3D supervisions, such as signed distances [53, 13, 41] and binary occupancy labels [48], or 2D supervisions, such as multi-view RGB images [60] and normal images [5]. In the following, we focus on reviewing methods of learning implicit representations from 2D and 3D supervisions separately. Then we provide a detailed discussion on the latest reconstruction methods based on 3D Gaussians.

2.1 Learning Implicit Representation from Multi-view Images

Neural radiance fields (NeRFs) [49] have become an essential technology for representing 3D scene through multi-view images. Many of its applications have been explored, resulting in significant advancements in areas such as acceleration [50, 12], dynamic scene [16, 4] and sparse rendering [58, 26]. Besides these applications, extracting accurate surfaces from NeRFs remains a challenge. Mainstream approaches typically design various differentiable formulas to transform the density in radiance fields into implicit representations for volume rendering, such as signed distance function (SDF) [60, 39, 54], unsigned distance function (UDF) [42, 47, 15, 70] and occupancy [52]. With the learned implicit function fields, post-processing algorithms [43, 21, 48] are applied to extract the zero level set to obtain the reconstructed meshes. Following methods introduce different priors from SfM [18, 69] or large-scale datasets [67, 59, 40] to improve the reconstruction performance in large-scale scenes. Recent approaches focus on speeding up the neural rendering procedure, aiming to achieve high-quality meshes and rendering views within a short period of training time. They

propose alternative data structures to replace the heavy MLP framework used in original NeRF, such as sparse voxel grid [17], multi-resolution hash grid [50, 61] and radial basis function [12], or design subtle differentiable rasterization pipelines to achieve real-time rendering [64, 56]. However, these methods still face the trade-off between rendering quality and training speed.

2.2 Learning Implicit Representation from Point Clouds

Since DeepSDF [53] and OccNet [48] were proposed, learning implicit representation from point clouds has achieved remarkable results in geometry modeling. These methods use ground truth signed distances and binary occupancy labels calculated from ground truth point clouds as supervisions to learn the implicit representation of shapes. The supervisions can serve as different kinds of global priors [3, 42, 55, 36] and local priors [62, 28, 38, 6], which enables the neural implicit function to better capture geometry details and generalize to unseen shapes during inference. Some other methods infer SDFs without 3D supervisions. They train neural networks to overfit on single point clouds. These methods introduce additional constraints [19, 76], novel ways of using gradients [45, 74, 51, 35, 75], specially designed priors [46, 10, 9] and normals [2, 37, 34] to estimate signed or unsigned distances and occupancy, which use point clouds as a reference.

2.3 Surface Reconstruction with 3D Gaussians

3D Gaussian Splatting [30] has become a new paradigm in neural rendering due to its fast rendering speed, intuitive explicit representation and outstanding rendering performance. However, reconstructing accurate surfaces from 3D Gaussian remains a challenge due to the messy, noisy, and unevenly distributed 3D Gaussians. To solve this problem, one kind of approaches involves combining 3D Gaussians with neural implicit surface functions [60, 50] to enhance the performance of both branches, which employs mutual supervisions between the two components [66, 11, 44]. Another kind of approaches encourage the reduction from 3D Gaussians to 2D Gaussians with a series of regularization terms, which ensures the Gaussian primitives to align with the object surfaces [25, 20, 14]. Additionally, some methods introduce additional priors from large-scale datasets [57, 14] or multi-view stereo [63], or use elaborately designed surface extraction algorithms [68, 65] to recover 3D geometry from 3D Gaussians. Although these efforts have achieved improved reconstructions, they are still limited in capturing fine-grained geometry and lack the precise perception of continuous implicit representations. Different from all these mentioned methods, we propose to seamlessly combine 3D Gaussians with the learning of neural SDFs. Our method provides a novel perspective to jointly learn 3D Gaussians and neural SDFs by more effectively using multi-view consistency and imposing geometry constraints.

3 Method

Overview. We aim to infer a neural SDF f from posed multi-view RGB images $\{v_i\}_{i=1}^I$, as shown in Fig. 1. We learn 3D Gaussian functions $\{g_j\}_{j=1}^J$ with their attributes like color, opacity, and shape to represent the geometry and color in the 3D scene. Meanwhile, when learning the 3D Gaussians, we introduce novel constraints to infer the continuous surfaces with the neural SDF. We rely on a differentiable pulling operation and the differentiable rasterization to bridge the gap between the discrete Gaussians and the continuous neural SDF, align 3D Gaussians on the zero-level set of the neural SDF, and back propagate the supervision signals from both the rendering errors and other geometry constraints to jointly optimize 3D Gaussians and the neural SDF.

Neural Signed Distance Function. We leverage an SDF f to represent the geometry of a scene. An SDF f is an implicit function that can predict a signed distance s at an arbitrary location q , i.e., $s = f(q)$. Recent methods usually train a neural network to approximate an SDF from signed distance supervision or infer an SDF from 3D point clouds or multi-view images. A level set is an iso-surface formed by the points with the same signed distance values. The zero-level set is a special level set, which is formed by points with a signed distance of 0. We can use the marching cubes algorithm [43] to extract the zero-level set as a mesh surface. Another character of the zero-level set is that the gradient of the SDF f at query q on the zero-level set, i.e., $\nabla f(q)$, is the normal of q .

3D Gaussian Splatting. 3D Gaussians have become a vital differentiable volume representation for scene modeling. We can learn a set of 3D Gaussians $\{g_j\}_{j=1}^J$, each of which has a set of learnable

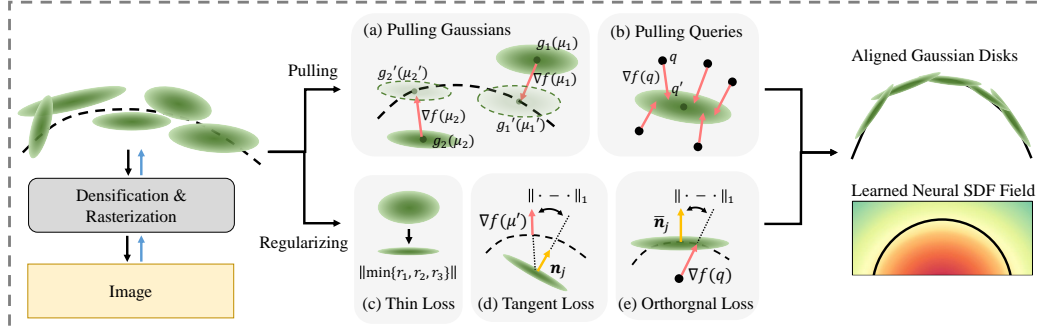


Figure 1: Overview of our method. We **(a)** pull 3D Gaussians onto the zero-level set for splatting, while **(b)** pulling the neighboring space onto the Gaussian disks for SDF inference. To better facilitate this procedure, we introduce three constraints: **(c)** push the Gaussians to become disks; **(d)** encourage the disk to be a tangent plane on the zero-level set; **(e)** constrain the query points to be pulled along the shortest path.

attributes including mean, variances, rotation, opacity, and color. We can render the learnable Gaussians $\{g_j\}$ into RGB images through the volume rendering equation below,

$$\mathbf{C}'(u, v) = \sum_{j=1}^J \mathbf{c}_j * o_j * p_j(u, v) \prod_{k=1}^{j-1} (1 - o_k * p_k(u, v)), \quad (1)$$

where $\mathbf{C}'(u, v)$ is the rendered color at the pixel (u, v) , \mathbf{c}_i , o_i , and p_i denote the color, the opacity, and the 2D projection of the j -th 3D Gaussian, respectively. At a query $q = [x, y, z]$, the probability from the j -th 3D Gaussian is $p_j(q) = \exp(-0.5 * (q - \mu_j)^T \Sigma^{-1}(q - \mu_j))$, where μ_j is the center of the j -th Gaussian, and Σ is the covariance matrix.

We can learn these 3D Gaussian functions through a differentiable rasterization. We render 3D Gaussians $\{g_j\}$ into rendered RGB images v'_i , and then, optimize the learnable attributes by minimizing the rendering errors to the ground truth observations v_i , where $\mathbf{C}'(u, v)$ and $\mathbf{C}(u, v)$ are the rendered and the GT color values at pixel (u, v) , i.e., $\min_{\{g_j\}} \|\mathbf{C}'(u, v) - \mathbf{C}(u, v)\|_2^2$.

Aligning 3D Gaussians with the Zero-level Set. Since 3D Gaussian splatting is so flexible in volume rendering, it does not require 3D Gaussians to locate on the geometry surface for good rendering quality. While we expect 3D Gaussians to locate on geometry surface, so that we can more effectively leverage them and multi-view consistency as clues to infer more accurate neural SDFs for reconstruction. To this end, we introduce a differentiable pulling operation to pull 3D Gaussians on the zero-level set of the neural SDF f , and then, we render the pulled 3D Gaussians through the splatting.

Specifically, inspired by Neural-Pull [45], we rely on the gradient field of the neural SDF f during the pulling operation. We move each one of the 3D Gaussians g_j using the predicted signed distance $s_j = f(\mu_j)$ and the gradient $\nabla f(\mu_j)$, where μ_j is the mean value of the 3D Gaussian. As shown in Fig. 1 (a), this pulling operation will turn the 3D Gaussian g_j into a 3D Gaussian g'_j that get projected onto the zero-level set of SDF f , where g'_j shares the same attributes with g_j but has a different center μ'_j ,

$$\mu'_j = \mu_j - s_j * \frac{\nabla f(\mu_j)}{|\nabla f(\mu_j)|}. \quad (2)$$

Signed Distance Inference with Pulled 3D Gaussians. We infer signed distances in the field with pulled 3D Gaussians $\{g'_j\}$. Pulled 3D Gaussians provide a coarse estimation of the surface, which we can use as a reference. One challenge here is that the sparsity and non-uniformly distributed 3D Gaussians do not show a clear geometry clue for surface inference. Although previous methods like NeuralTPS [8] and OnSurfPrior [46] manage to learn continuous implicit functions from sparse points, it is still difficult to recover surfaces from both sparse and non-uniformly distributed points.

To overcome this challenge, we introduce an approach to estimate neural SDFs from sparse 3D Gaussians. Like Neural-Pull [45], we still use a differentiable pulling operation to pull neighboring space onto the surface but we regard the disk established by the shape of a 3D Gaussian as a pulling target, rather than a point, as shown in Fig. 2, which aims for a larger target on surfaces. To this end, we impose constraints not only on the shape of 3D Gaussians but also on the pulling operation. Specifically, we introduce three constraints. The first one constrains 3D Gaussians to be a thin disk. The second constraint encourages the thin disk to be a tangent plane on the zero-level set. The third constraint pushes queries to get pulled onto the thin disk along the normal of the Gaussian.

The first constraint adds penalties if the smallest variance among the three variances of a 3D Gaussian g_j is too large, as shown in Fig. 1 (c). Thus, the loss for a thin disk Gaussian is listed below,

$$L_{Thin} = \|\min\{r_1, r_2, r_3\}\|_1, \quad (3)$$

where r_1 , r_2 , and r_3 are variances along the three axes. Flattening a 3D Gaussian ellipsoid into a disk was first introduced in NeuSG [11] and has become a consensus in recent Gaussian reconstruction works [25, 14]. The motivation is that 2D planar disk primitives are more suitable for surface representation, making it easier to apply alignment constraints. Additionally, we can naturally use the direction pointing along the axis with the minimum variance $\bar{r} = \min\{r_1, r_2, r_3\}$ to represent the normal n_j of the Gaussian g_j .

Based on the thin disk shape of Gaussians, the second constraint encourages the pulled Gaussians $\{g'_j\}$ to be the tangent plane on the zero-level set, as shown in Fig. 1 (d). What we do is to align the normal n_j of a Gaussian g_j with the normal at the center μ'_j of the pulled Gaussian g'_j on the zero-level set. We use the gradient $\nabla f(\mu'_j)$ of the neural SDF at μ'_j as the expected normal here. Hence, we align the normal n_j of a Gaussian with the normal $\nabla f(\mu'_j)$ on the zero-level set,

$$L_{Tangent} = 1 - \left| \frac{\nabla f(\mu'_j)}{|\nabla f(\mu'_j)|} \cdot n_j \right| \quad (4)$$

With the disk-like Gaussians located on the tangent plane, we introduce to sense the signed distance field by pulling randomly sampled queries on the Gaussian disks, as shown in Fig. 1 (b). Turning the pulling target from a point [45, 8] into a plane is based on the observation that the 3D Gaussian function with a boundary can cover the surface more completely although their centers $\{\mu_1, \dots, \mu_j\}$ which are sparse and non-uniformly distributed. Thus, we expect the operation can pull a query onto a Gaussian disk plane. Fig. 2 demonstrates the improvement of pulling queries onto their nearest Gaussian disk planes over the nearest Gaussian centers. The comparisons show that pulling onto the disk plane can improve the robustness to the sparsity and non-uniformly Gaussian distribution. With learned Gaussian centers, pulling queries to centers can not recover the smooth and continuous geometry in areas where almost no Gaussian centers appear. While pulling queries to the Gaussian disk plane can recover more accurate and complete surfaces since the disk established by the learned variance of Gaussian functions can mostly cover the gap.

Specifically, at a query q , we pull it onto the zero-level set using a similar way in Eq. 2, i.e., $q' = q - s * \nabla f(q)/|\nabla f(q)|$. To encourage the query to get pulled onto the nearest pulled Gaussian disk, we maximize its probability of belonging to its nearest pulled Gaussian \bar{g} which is determined in terms of the distance between q and the Gaussian center $\bar{\mu}$,

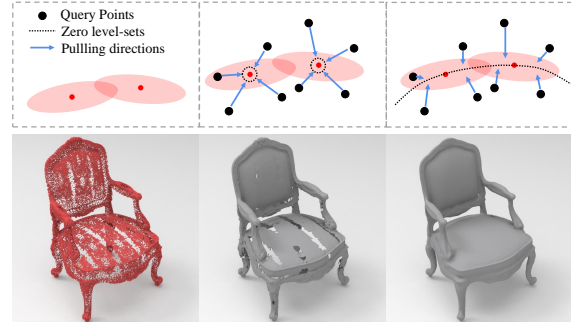


Figure 2: Comparison of pulling Gaussians to centers and to disks. The former tends to overfit sparse Gaussian centers, resulting in incomplete meshes. We address this issue by pulling queries onto disk planes.

$$L_{Pull}(q'; \bar{\mu}) = e^{-1/2*(q' - \bar{\mu})^T \Sigma^{-1}(q' - \bar{\mu})}, \bar{g} = \arg \min_{\{g'_j\}} ||\mu'_j - q||_2^2. \quad (5)$$

We minimize the negative logarithm of the probability in our implementation. Moreover, we expect the pulling can follow a direction orthogonal to the disk plane, which leads to the minimum moving distance conform to the definition of signed distances. To this end, we impose another constraint on the gradient to ensure that the pulling can follow a path with the minimum distance to the nearest pulled Gaussian disk, as shown in Fig. 1 (e),

$$L_{Orthogonal} = 1 - \left| \frac{\nabla f(q)}{|\nabla f(q)|} \cdot \bar{n}_j \right|, \quad (6)$$

where the constraint aligns the gradient at query q and the normal \bar{n}_j of the pulled Gaussian disk \bar{g} .

Rendering. We also render the pulled Gaussians $\{g'_j\}$ into images through splatting to add penalties on rendering errors, where $\{g'_j\}$ are Gaussians pulled onto the zero-level set from the Gaussians $\{g_j\}$ by the neural SDF f in Eq. 2. Each pair of g_j and g'_j shares the same attributes except the center location. The rendering error combines an L_1 term and a D-SSIM term between rendered images $\{v'_i\}_{i=1}^I$ and ground truth ones $\{v_i\}_{i=1}^I$, following original 3DGS [30],

$$L_{Splatting} = 0.8 \cdot L_1(v'_i, v_i) + 0.2 \cdot L_{D-SSIM}(v'_i, v_i). \quad (7)$$

Loss Function. We optimize attributes of Gaussians $\{g_j\}$ and the parameters of neural SDF f by the following objective function, where α, β, γ , and δ are balance weights.

$$\min_{\{g_j\}, f} L_{Splatting} + \alpha L_{Thin} + \beta L_{Tangent} + \gamma L_{Pull} + \delta L_{Orthogonal}. \quad (8)$$

Implementation Details. Our code is build upon the source code released by 3DGS [30]. Similar to [68], we make some changes to 3DGS’s densification strategy. The first one is to initialize the newly cloned Gaussians around the original Gaussians rather than at the same positions. The second one is to encourage 3DGS to split larger Gaussians into smaller ones more frequently. These strategies aim to increase the number of primitives and to avoid underfitting in textureless areas. Regularization parameters are set to $\alpha=100, \beta=0.1, \gamma=1, \delta=0.1$. We optimize our model for a total of 15k iterations. We stop densification and incorporate the pulling and constraints at 7k iterations. The SDF network is implemented as an MLP with 8 layers, 256 hidden units and ReLU activation function, and initialized as a sphere, following [45]. The parameters of the SDF network shares the same optimizer as that of 3D Gaussians. All the experiments are conducted on a single NVIDIA 3090 GPU.

4 Experiments

4.1 Experiment Settings

Evaluation Metrics and Datasets. We evaluate the performance of our method on widely adopted datasets including both object-level and large-scale ones, including DTU [27], Tanks and Temples (TNT) [31] and Mip-NeRF 360 (M360) [1]. To evaluate the accuracy of the reconstructed meshes, we use Chamfer Distance (CD) on DTU and F-score on TNT, using the official evaluation script. To evaluate the rendering quality in real-scene datasets, we report PSNR, SSIM and LPIPS in evaluations on M360.

Baselines. We compare our geometry reconstruction accuracy with the state-of-the-art 3DGS based reconstruction methods, including SuGaR [20], DN-Splatter [57], GaussianSurfels [14] and 2DGS [25]. For real-world scenes which do not have ground truth meshes for evaluations, we compare the rendering quality with state-of-the-art neural rendering methods, including Instant-NGP [50], Mip-NeRF 360 [1] and BakedSDF [64].

Surface Extraction. An advantage of our approach over the latest methods is the simplicity of extracting surfaces. Different from methods like SuGaR [20] and GauS [65] which introduce

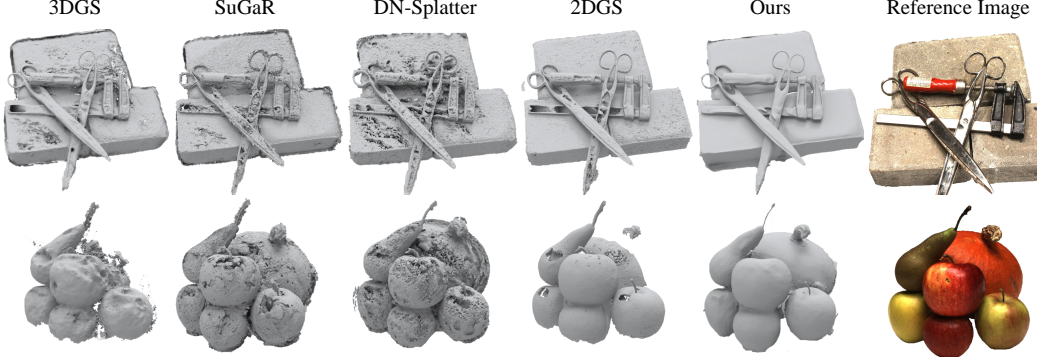


Figure 3: Visual comparisons on DTU dataset.

Table 1: Numerical comparisons in terms of CD on DTU dataset. Best results are highlighted as 1st, 2nd and 3rd.

Methods	24	37	40	55	63	65	69	83	97	105	106	110	114	118	122	Mean	Time
NeuS [60]	1.00	1.37	0.93	0.43	1.10	0.65	0.57	1.48	1.09	0.83	0.52	1.20	0.35	0.49	0.54	0.84	~9h
3DGS [30]	2.14	1.53	2.08	1.68	3.49	2.21	1.43	2.07	2.22	1.75	1.79	2.55	1.53	1.52	1.50	1.96	15.1m
SuGaR [20]	1.47	1.33	1.13	0.61	2.25	1.71	1.15	1.63	1.62	1.07	0.79	2.45	0.98	0.88	0.79	1.33	1.6h
DN-Splatter [57]	1.60	2.03	1.42	1.44	2.37	2.11	1.62	1.95	1.88	1.48	1.63	1.82	1.20	1.50	1.40	1.70	31.2m
GSurfels [14]	0.66	0.93	0.54	0.41	1.06	1.14	0.85	1.29	1.53	0.79	0.82	1.58	0.45	0.66	0.53	0.88	10.9m
2DGS [25]	0.48	0.91	0.39	0.39	1.01	0.83	0.81	1.36	1.27	0.76	0.70	1.40	0.40	0.76	0.52	0.80	20.5m
Ours	0.51	0.56	0.46	0.39	0.82	0.67	0.85	1.37	1.25	0.73	0.54	1.39	0.35	0.88	0.42	0.75	21.8m

Table 2: Numerical comparisons on Tanks And Temples dataset. Best results are highlighted as 1st, 2nd and 3rd.

Methods	Barn	Caterpillar	Courthouse	Ignatius	Meetingroom	Truck	Mean	Time
NeuS [60]	0.29	0.29	0.17	0.83	0.24	0.45	0.38	~12h
3DGS [30]	0.13	0.08	0.09	0.04	0.01	0.19	0.09	20.5m
SuGaR [20]	0.14	0.16	0.08	0.33	0.15	0.26	0.19	2.1h
DN-Splatter [57]	0.15	0.11	0.07	0.18	0.01	0.20	0.12	54.9m
GSurfels [14]	0.24	0.22	0.07	0.39	0.12	0.24	0.21	15.1m
2DGS [25]	0.41	0.23	0.16	0.51	0.17	0.45	0.32	39.4m
Ours	0.60	0.37	0.16	0.71	0.22	0.52	0.43	37.6m

specially designed algorithms and take a long time for extracting surfaces, we adopt the marching cubes algorithm [43] to extract mesh surfaces with the learned neural SDF f . For small scale scenes, we use a resolution of 800 to extract surfaces, while we split large scale scenes into parts, each of which gets reconstructed with a resolution of 800 to bypass the limitation of our computational resources.

4.2 Comparisons

Comparisons on DTU. We report accuracy of reconstructed meshes and training time against baselines on DTU dataset in Tab. 1. Our method outperforms all Gaussian-based reconstruction methods in terms of Chamfer Distance. Our method achieves comparable training time to the state-of-the-art Gaussian-reconstruction method 2DGS [25] but gains better reconstruction accuracy than 2DGS. The visualization results in Fig. 3 highlight the advantages of our method. By employing alignment constraints and pulling operations between the 3D Gaussians and the neural SDF field, we can reconstruct significantly smoother and more complete surfaces than the baselines.

Comparisons on TNT. We further evaluate our method using more challenging large-scale unbounded scenes on TNT dataset. Numerical comparisons in Tab. 2 show that we achieve higher F-score compared to baseline methods, even surpassing NeuS, which however takes about 12 hours to fit a scene. Notably, as the scene scale increases, the number of Gaussian primitives increases rapidly, causing the adjusted CUDA rasterization kernel of 2DGS to consume more time for rendering. In contrast, since our rasterization kernel is based on 3DGS, it is less sensitive to the number of Gaussians, which enables us to learn 3D Gaussians faster than 2DGS. We provide visual comparisons



Figure 4: Visual comparisons on Tanks and Temples dataset.

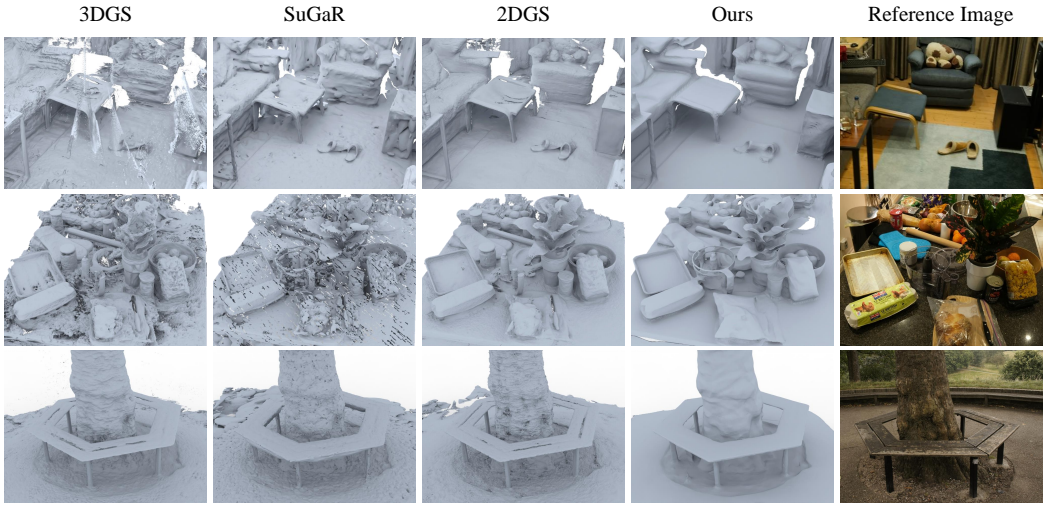


Figure 5: Visual comparisons on Mip-NeRF 360 dataset.

in Fig. 4. Here we crop the reconstructed meshes to show the foreground objects that are of primary interest, as captured by the cameras. Please refer to the appendix for the reconstruction results of the background regions. The visual comparisons demonstrate that we can reconstruct more complete and smooth object surfaces, such as the ground, the truck’s hood and the statue’s left shoulder.

Comparisons on Mip-NeRF 360. We further evaluate our method in neural rendering for novel view synthesis on MipNeRF 360 dataset. We report the numerical comparisons in Tab. 3. Our competitive results against the state-of-the-art novel view synthesis methods indicate that our method is able to impose effective geometric constraints without compromising rendering quality. This provides a promising solution for learning continuous distance fields from discrete 3D Gaussians. Visual comparisons of mesh reconstructions are shown in Fig. 5, which demonstrate that our method is able to recover more smooth and complete surface by more effectively using the multi-view consistency.

Table 3: Quantitative evaluations of rendering quality on Mip-NeRF 360 [1] dataset. Best results are highlighted as 1st, 2nd and 3rd.

	Indoor Scene			Outdoor Scene		
	PSNR↑	SSIM↑	LPIPS↓	PSNR↑	SSIM↑	LPIPS↓
NeRF[49]	26.84	0.790	0.370	21.46	0.458	0.515
Instant-NGP [50]	29.15	0.880	0.216	22.90	0.566	0.371
MipNeRF 360 [1]	31.72	0.917	0.180	24.47	0.691	0.283
BakedSDF [64]	27.06	0.839	0.258	22.47	0.585	0.349
3DGS [30]	30.99	0.926	0.199	24.24	0.705	0.283
SuGaR [20]	29.44	0.911	0.216	22.76	0.631	0.349
2DGS [25]	30.39	0.924	0.183	24.33	0.709	0.284
Ours	30.78	0.925	0.182	23.76	0.703	0.278

Table 4: Ablation studies on DTU dataset.

Methods	Pulling		Constraint Terms			Mesh Extractions		
	Pulled to centers	w/o Pull GS	w/o L_{Thin}	w/o L_{Tan}	w/o L_{Oth}	TSDF	Poisson	Full model
CD↓	0.85	0.90	0.78	0.82	0.79	1.41	0.79	0.75

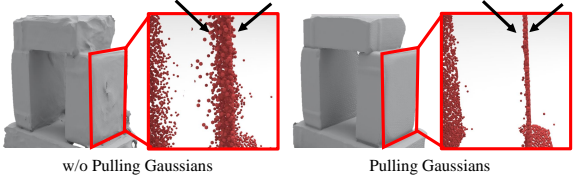
4.3 Ablation Studies

In this section, we conduct ablation studies on the key techniques of our method to demonstrate their effectiveness. The full quantitative results are reported in Tab. 4, which are conducted on all scenes in DTU dataset [27].

Pulling Operations. We first examine the effect of pulling Gaussians onto the zero-level set, as reported in Tab. 4 ("w/o Pull Gaussians" vs. "Ours"). The original 3DGS tends to produce floating ellipsoids near the object surfaces to overfit the training views. By pulling the Gaussians to the zero-level set of the SDF field, the Gaussians are consistently distributed on the surface. As shown in Fig. 6a, after getting pulled onto the zero-level set, the Gaussian centers are distributed on a thin layer of the object surface, thus achieving an accurate geometry estimation. Meanwhile, we pull neighboring space onto Gaussian disks to learn neural SDFs. Comparing to NeuralPull [45] which pulls query points to centers, we innovatively pull query points to Gaussian disks, which bridge the gap between continuous SDF field and sparse Gaussian distributions, as highlighted in Fig. 2 and Tab. 4 ("Pulled to centers" vs. "Ours").

Constraint Terms. We further explore the effect of our constraint terms, as reported in Tab. 4 ("Constraint Terms"). Our full model provides the best performance when applying all constraint terms. The orthogonal loss helps to learn a more regularized SDF field, while the thin loss and tangent loss provide constraints to align the orientation of Gaussian disks with the gradient of neural SDF on the zero-level sets, resulting in a good normal field and a reconstructed mesh, as shown in Fig. 6b, 6c.

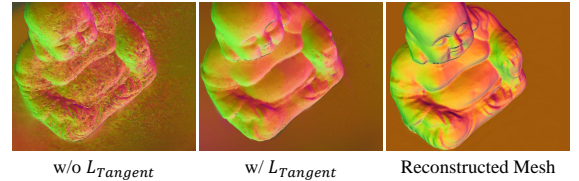
Mesh Extraction. We also report the reconstruction accuracy using TSDF fusion and screened Poisson reconstruction [29], as shown in Fig. 6d and Tab. 4 ("Mesh Extractions"). For TSDF fusion, we render depth maps and fuse them using a voxel size of 0.004 and truncation threshold as 0.02, the same as 2DGS [25]. For screened Poisson, we use the Gaussian centers and normals as input. Unlike 2DGS [25] and GSurfels [14] which incorporate rendered depth into the differentiable rasterization pipeline, we do not directly optimize depths, resulting in noisy depth maps and unsatisfactory reconstruction results. However, since the positions and normals of the Gaussians are well optimized through our approach, screened Poisson reconstruction can achieve relatively good results.



(a) Visualization of Gaussian centers with or without pulled onto zero-level set. We are able to obtain consistent and smooth Gaussian distributions by pulling operation.



(b) Comparisons between Gaussian ellipsoids learned by original 3DGS and Gaussian disks learned by our method.



(c) Qualitative ablation studies for Tangent loss.



(d) Comparisons of different mesh extraction methods.

Gradient Constraint. We follow Neural-Pull [45] to use normalized SDF gradient for pulling operation. We report the result with an additional Eikonal term [19] to explicitly constrain the gradient length, as shown in Fig. 7. The result is significantly degenerated because that Neural-Pull depends on both predicted SDF values and gradient directions to optimize the SDF field. It makes the optimization even more complex when adding additional constraint on the gradient length.

5 Conclusion

We propose a method to learn neural SDFs for multi-view surface reconstruction with 3D Gaussian splatting. Our results show that we can more effectively leverage multi-view consistency to recover more accurate, smooth, and complete surfaces with geometry details by rendering 3D Gaussians pulled on the zero-level set. To this end, we dynamically align 3D Gaussians to the zero-level set and update neural SDFs through both differentiable pulling and splatting for both RGB and geometry constraints. Our methods successfully refine the signed distance field near the surface in a progressive manner, leading to plausible surface reconstruction. Our ablation studies justify the effectiveness of our novel modules, loss terms, and training strategies. Our evaluations show our superiority over the latest methods in terms of accuracy, completeness, and smoothness.

6 Acknowledgement

This work was supported by National Key R&D Program of China (2022YFC3800600), and the National Natural Science Foundation of China (62272263, 62072268), and in part by Tsinghua-Kuaishou Institute of Future Media Data.

References

- [1] Jonathan T. Barron, Ben Mildenhall, Dor Verbin, Pratul P. Srinivasan, and Peter Hedman. Mip-NeRF 360: Unbounded anti-aliased neural radiance fields. In *Proceedings of the IEEE Conference on Computer Vision and Pattern Recognition*, 2022.
- [2] Alexandre Boulch, Pierre-Alain Langlois, Gilles Puy, and Renaud Marlet. NeeDrop: Self-supervised shape representation from sparse point clouds using needle dropping. In *International Conference on 3D Vision*, 2021.
- [3] Alexandre Boulch and Renaud Marlet. POCO: Point convolution for surface reconstruction. In *IEEE Conference on Computer Vision and Pattern Recognition*, 2022.
- [4] Ang Cao and Justin Johnson. HexPlane: A fast representation for dynamic scenes. In *Proceedings of the IEEE/CVF Conference on Computer Vision and Pattern Recognition*, pages 130–141, 2023.
- [5] Xu Cao and Takafumi Taketomi. Supernormal: Neural surface reconstruction via multi-view normal integration. In *Proceedings of the IEEE/CVF Conference on Computer Vision and Pattern Recognition*, pages 20581–20590, 2024.
- [6] Chao Chen, Zhizhong Han, and Yu-Shen Liu. Learning local pattern modularization for point cloud reconstruction from unseen classes. In *European Conference on Computer Vision*, 2024.
- [7] Chao Chen, Yu-Shen Liu, and Zhizhong Han. GridPull: Towards scalability in learning implicit representations from 3d point clouds. In *Proceedings of the IEEE/CVF Conference on Computer Vision and Pattern Recognition*, pages 18322–18334, 2023.

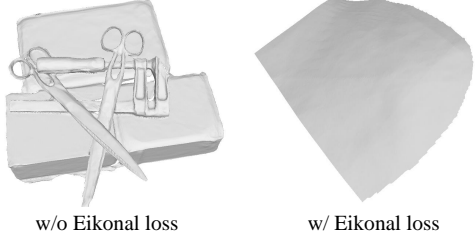


Figure 7: Visualization of the effect of eikonal loss.

- [8] Chao Chen, Yu-Shen Liu, and Zhizhong Han. Unsupervised inference of signed distance functions from single sparse point clouds without learning priors. In *Proceedings of the IEEE/CVF Conference on Computer Vision and Pattern Recognition*, pages 17712–17723, 2023.
- [9] Chao Chen, Yu-Shen Liu, and Zhizhong Han. Inferring neural signed distance functions by overfitting on single noisy point clouds through finetuning data-driven based priors. In *Advances in Neural Information Processing Systems*, 2024.
- [10] Chao Chen, Yu-Shen Liu, and Zhizhong Han. NeuralTPS: Learning signed distance functions without priors from single sparse point clouds. *IEEE Transactions on Pattern Analysis and Machine Intelligence*, 2024.
- [11] Hanlin Chen, Chen Li, and Gim Hee Lee. NeuSG: Neural Implicit Surface Reconstruction with 3D Gaussian Splatting Guidance. *arXiv preprint arXiv:2312.00846*, 2023.
- [12] Zhang Chen, Zhong Li, Liangchen Song, Lele Chen, Jingyi Yu, Junsong Yuan, and Yi Xu. NeuRBF: A neural fields representation with adaptive radial basis functions. In *Proceedings of the IEEE/CVF International Conference on Computer Vision*, pages 4182–4194, 2023.
- [13] Gene Chou, Ilya Chugunov, and Felix Heide. GenSDF: Two-Stage Learning of Generalizable Signed Distance Functions. In *Advances in Neural Information Processing Systems*, 2022.
- [14] Pinxuan Dai, Jiamin Xu, Wenxiang Xie, Xinguo Liu, Huamin Wang, and Weiwei Xu. High-quality surface reconstruction using gaussian surfels. In *SIGGRAPH 2024 Conference Papers*. Association for Computing Machinery, 2024.
- [15] Junkai Deng, Fei Hou, Xuhui Chen, Wencheng Wang, and Ying He. 2S-UDF: A Novel Two-stage UDF Learning Method for Robust Non-watertight Model Reconstruction from Multi-view Images. 2024.
- [16] Sara Fridovich-Keil, Giacomo Meanti, Frederik Rahbæk Warburg, Benjamin Recht, and Angjoo Kanazawa. K-Planes: Explicit radiance fields in space, time, and appearance. In *Proceedings of the IEEE/CVF Conference on Computer Vision and Pattern Recognition*, pages 12479–12488, 2023.
- [17] Sara Fridovich-Keil, Alex Yu, Matthew Tancik, Qinhong Chen, Benjamin Recht, and Angjoo Kanazawa. Plenoxels: Radiance fields without neural networks. In *Proceedings of the IEEE/CVF Conference on Computer Vision and Pattern Recognition*, pages 5501–5510, 2022.
- [18] Qiancheng Fu, Qingshan Xu, Yew-Soon Ong, and Wenbing Tao. Geo-Neus: Geometry-consistent neural implicit surfaces learning for multi-view reconstruction. In *Advances in Neural Information Processing Systems*, 2022.
- [19] Amos Gropp, Lior Yariv, Niv Haim, Matan Atzmon, and Yaron Lipman. Implicit geometric regularization for learning shapes. In *International Conference on Machine Learning*, pages 3789–3799. PMLR, 2020.
- [20] Antoine Guédon and Vincent Lepetit. SuGaR: Surface-aligned gaussian splatting for efficient 3d mesh reconstruction and high-quality mesh rendering. *Proceedings of the IEEE/CVF Conference on Computer Vision and Pattern Recognition*, 2024.
- [21] Benoit Guillard, Federico Stella, and Pascal Fua. MeshUDF: Fast and differentiable meshing of unsigned distance field networks. In *European Conference on Computer Vision*, pages 576–592. Springer, 2022.
- [22] Yasaman Haghighi, Suryansh Kumar, Jean-Philippe Thiran, and Luc Van Gool. Neural Implicit Dense Semantic SLAM. *arXiv preprint arXiv:2304.14560*, 2023.
- [23] Liang Han, Junsheng Zhou, Yu-Shen Liu, and Zhizhong Han. Binocular-guided 3d gaussian splatting with view consistency for sparse view synthesis. In *Advances in Neural Information Processing Systems*, 2024.

- [24] Pengchong Hu and Zhizhong Han. Learning neural implicit through volume rendering with attentive depth fusion priors. In *Advances in Neural Information Processing Systems*, 2023.
- [25] Binbin Huang, Zehao Yu, Anpei Chen, Andreas Geiger, and Shenghua Gao. 2D Gaussian Splatting for Geometrically Accurate Radiance Fields. In *SIGGRAPH 2024 Conference Papers*. Association for Computing Machinery, 2024.
- [26] Han Huang, Yulun Wu, Junsheng Zhou, Ge Gao, Ming Gu, and Yu-Shen Liu. NeuSurf: On-surface priors for neural surface reconstruction from sparse input views. In *Proceedings of the AAAI Conference on Artificial Intelligence*, volume 38, pages 2312–2320, 2024.
- [27] Rasmus Jensen, Anders Dahl, George Vogiatzis, Engil Tola, and Henrik Aanæs. Large scale multi-view stereopsis evaluation. In *IEEE Conference on Computer Vision and Pattern Recognition*, pages 406–413, 2014.
- [28] Chiyu Jiang, Avneesh Sud, Ameesh Makadia, Jingwei Huang, Matthias Nießner, Thomas Funkhouser, et al. Local implicit grid representations for 3D scenes. In *Proceedings of the IEEE/CVF Conference on Computer Vision and Pattern Recognition*, pages 6001–6010, 2020.
- [29] Michael Kazhdan and Hugues Hoppe. Screened poisson surface reconstruction. *ACM Transactions on Graphics (ToG)*, 32(3):1–13, 2013.
- [30] Bernhard Kerbl, Georgios Kopanas, Thomas Leimkühler, and George Drettakis. 3D gaussian splatting for real-time radiance field rendering. *ACM Transactions on Graphics*, 42(4):1–14, 2023.
- [31] Arno Knapitsch, Jaesik Park, Qian-Yi Zhou, and Vladlen Koltun. Tanks and Temples: Benchmarking large-scale scene reconstruction. *ACM Transactions on Graphics*, 36(4), 2017.
- [32] Xin Kong, Shikun Liu, Marwan Taher, and Andrew J Davison. vMAP: Vectorised object mapping for neural field slam. In *Proceedings of the IEEE/CVF Conference on Computer Vision and Pattern Recognition*, pages 952–961, 2023.
- [33] A. Laurentini. The visual hull concept for silhouette-based image understanding. *IEEE Transactions on Pattern Analysis and Machine Intelligence*, 16(2):150–162, 1994.
- [34] Qing Li, Huifang Feng, Kanle Shi, Yue Gao, Yi Fang, Yu-Shen Liu, and Zhizhong Han. Learning signed hyper surfaces for oriented point cloud normal estimation. *IEEE Transactions on Pattern Analysis and Machine Intelligence*, 2024.
- [35] Shengtao Li, Ge Gao, Yudong Liu, Ming Gu, and Yu-Shen Liu. Implicit filtering for learning neural signed distance functions from 3d point clouds. *European Conference on Computer Vision*, 2024.
- [36] Shengtao Li, Ge Gao, Yudong Liu, Yu-Shen Liu, and Ming Gu. GridFormer: Point-grid transformer for surface reconstruction. In *Proceedings of the AAAI Conference on Artificial Intelligence*, volume 38, pages 3163–3171, 2024.
- [37] Shujuan Li, Junsheng Zhou, Baorui Ma, Yu-Shen Liu, and Zhizhong Han. NeAF: Learning neural angle fields for point normal estimation. In *Proceedings of the AAAI Conference on Artificial Intelligence*, volume 37, pages 1396–1404, 2023.
- [38] Shujuan Li, Junsheng Zhou, Baorui Ma, Yu-Shen Liu, and Zhizhong Han. Learning continuous implicit field with local distance indicator for arbitrary-scale point cloud upsampling. In *Proceedings of the AAAI Conference on Artificial Intelligence*, volume 38, pages 3181–3189, 2024.
- [39] Zhaoshuo Li, Thomas Müller, Alex Evans, Russell H Taylor, Mathias Unberath, Ming-Yu Liu, and Chen-Hsuan Lin. Neuralangelo: High-fidelity neural surface reconstruction. In *Proceedings of the IEEE/CVF Conference on Computer Vision and Pattern Recognition*, pages 8456–8465, 2023.

- [40] Zhihao Liang, Zhangjin Huang, Changxing Ding, and Kui Jia. HelixSurf: A robust and efficient neural implicit surface learning of indoor scenes with iterative intertwined regularization. In *Proceedings of the IEEE/CVF Conference on Computer Vision and Pattern Recognition*, pages 13165–13174, 2023.
- [41] David B Lindell, Dave Van Veen, Jeong Joon Park, and Gordon Wetzstein. Bacon: Band-limited coordinate networks for multiscale scene representation. In *Proceedings of the IEEE/CVF conference on computer vision and pattern recognition*, pages 16252–16262, 2022.
- [42] Xiaoxiao Long, Cheng Lin, Lingjie Liu, Yuan Liu, Peng Wang, Christian Theobalt, Taku Komura, and Wenping Wang. NeuralUDF: Learning unsigned distance fields for multi-view reconstruction of surfaces with arbitrary topologies. In *Proceedings of the IEEE/CVF Conference on Computer Vision and Pattern Recognition*, pages 20834–20843, 2023.
- [43] William E. Lorensen and Harvey E. Cline. Marching cubes: A high resolution 3D surface construction algorithm. *Computer Graphics*, 21(4):163–169, 1987.
- [44] Xiaoyang Lyu, Yang-Tian Sun, Yi-Hua Huang, Xiuzhe Wu, Ziyi Yang, Yilun Chen, Jiangmiao Pang, and Xiaojuan Qi. 3DGSR: Implicit Surface Reconstruction with 3D Gaussian Splatting. *arXiv preprint arXiv:2404.00409*, 2024.
- [45] Baorui Ma, Zhizhong Han, Yu-Shen Liu, and Matthias Zwicker. Neural-Pull: Learning signed distance function from point clouds by learning to pull space onto surface. In *International Conference on Machine Learning*, pages 7246–7257. PMLR, 2021.
- [46] Baorui Ma, Yu-Shen Liu, Matthias Zwicker, and Zhizhong Han. Reconstructing surfaces for sparse point clouds with on-surface priors. In *IEEE Conference on Computer Vision and Pattern Recognition*, 2022.
- [47] Xiaoxu Meng, Weikai Chen, and Bo Yang. NeAT: Learning neural implicit surfaces with arbitrary topologies from multi-view images. In *Proceedings of the IEEE/CVF Conference on Computer Vision and Pattern Recognition*, pages 248–258, 2023.
- [48] Lars Mescheder, Michael Oechsle, Michael Niemeyer, Sebastian Nowozin, and Andreas Geiger. Occupancy networks: Learning 3D reconstruction in function space. In *Proceedings of the IEEE/CVF Conference on Computer Vision and Pattern Recognition*, pages 4460–4470, 2019.
- [49] Ben Mildenhall, Pratul P Srinivasan, Matthew Tancik, Jonathan T Barron, Ravi Ramamoorthi, and Ren Ng. NeRF: Representing scenes as neural radiance fields for view synthesis. In *European Conference on Computer Vision (ECCV)*, pages 405–421. Springer, 2020.
- [50] Thomas Müller, Alex Evans, Christoph Schied, and Alexander Keller. Instant neural graphics primitives with a multiresolution hash encoding. *ACM Transactions on Graphics (ToG)*, 41(4):1–15, 2022.
- [51] Takeshi Noda, Chao Chen, Weiqi Zhang, Xinhai Liu, Yu-Shen Liu, and Zhizhong Han. MultiPull: Detailing signed distance functions by pulling multi-level queries at multi-step. In *Advances in Neural Information Processing Systems*, 2024.
- [52] Michael Oechsle, Songyou Peng, and Andreas Geiger. UNISURF: Unifying neural implicit surfaces and radiance fields for multi-view reconstruction. In *Proceedings of the IEEE/CVF International Conference on Computer Vision*, pages 5589–5599, 2021.
- [53] Jeong Joon Park, Peter Florence, Julian Straub, Richard Newcombe, and Steven Lovegrove. DeepSDF: Learning continuous signed distance functions for shape representation. In *Proceedings of the IEEE/CVF Conference on Computer Vision and Pattern Recognition*, pages 165–174, 2019.
- [54] Minyoung Park, Mirae Do, Yeon Jae Shin, Jaeseok Yoo, Jongkwang Hong, Joongrock Kim, and Chul Lee. H2O-SDF: Two-phase learning for 3d indoor reconstruction using object surface fields. In *The Twelfth International Conference on Learning Representations*, 2023.

- [55] Songyou Peng, Michael Niemeyer, Lars Mescheder, Marc Pollefeys, and Andreas Geiger. Convolutional occupancy networks. In *European Conference on Computer Vision*, pages 523–540. Springer, 2020.
- [56] Christian Reiser, Rick Szeliski, Dor Verbin, Pratul Srinivasan, Ben Mildenhall, Andreas Geiger, Jon Barron, and Peter Hedman. MeRF: Memory-efficient radiance fields for real-time view synthesis in unbounded scenes. *ACM Transactions on Graphics (TOG)*, 42(4):1–12, 2023.
- [57] Matias Turkulainen, Xuqian Ren, Iaroslav Melekhov, Otto Seiskari, Esa Rahtu, and Juho Kannala. DN-Splatter: Depth and normal priors for gaussian splatting and meshing. *arXiv preprint arXiv:2403.17822*, 2024.
- [58] Guangcong Wang, Zhaoxi Chen, Chen Change Loy, and Ziwei Liu. SparseNeRF: Distilling depth ranking for few-shot novel view synthesis. In *Proceedings of the IEEE/CVF International Conference on Computer Vision*, pages 9065–9076, 2023.
- [59] Jiepeng Wang, Peng Wang, Xiaoxiao Long, Christian Theobalt, Taku Komura, Lingjie Liu, and Wenping Wang. NeuRIS: Neural reconstruction of indoor scenes using normal priors. In *European Conference on Computer Vision*, 2022.
- [60] Peng Wang, Lingjie Liu, Yuan Liu, Christian Theobalt, Taku Komura, and Wenping Wang. NeuS: Learning neural implicit surfaces by volume rendering for multi-view reconstruction. *Advances in Neural Information Processing Systems*, 34, 2021.
- [61] Yiming Wang, Qin Han, Marc Habermann, Kostas Daniilidis, Christian Theobalt, and Lingjie Liu. NeuS2: Fast learning of neural implicit surfaces for multi-view reconstruction. In *Proceedings of the IEEE/CVF International Conference on Computer Vision*, pages 3295–3306, 2023.
- [62] Francis Williams, Teseo Schneider, Claudio Silva, Denis Zorin, Joan Bruna, and Daniele Panozzo. Deep geometric prior for surface reconstruction. In *IEEE Conference on Computer Vision and Pattern Recognition*, 2019.
- [63] Yaniv Wolf, Amit Bracha, and Ron Kimmel. Surface reconstruction from gaussian splatting via novel stereo views. *European Conference on Computer Vision*, 2024.
- [64] Lior Yariv, Peter Hedman, Christian Reiser, Dor Verbin, Pratul P Srinivasan, Richard Szeliski, Jonathan T Barron, and Ben Mildenhall. Bakedsdf: Meshing neural sdf’s for real-time view synthesis. In *ACM SIGGRAPH 2023 Conference Proceedings*, pages 1–9, 2023.
- [65] Chongjie Ye, Yinyu Nie, Jiahao Chang, Yuantao Chen, Yihao Zhi, and Xiaoguang Han. GauStudio: A Modular Framework for 3D Gaussian Splatting and Beyond. *arXiv preprint arXiv:2403.19632*, 2024.
- [66] Mulin Yu, Tao Lu, Linning Xu, Lihan Jiang, Yuanbo Xiangli, and Bo Dai. GSDF: 3DGS Meets SDF for Improved Rendering and Reconstruction. *arXiv preprint arXiv:2403.16964*, 2024.
- [67] Zehao Yu, Songyou Peng, Michael Niemeyer, Torsten Sattler, and Andreas Geiger. MonoSDF: Exploring monocular geometric cues for neural implicit surface reconstruction. *Advances in Neural Information Processing Systems*, 2022.
- [68] Zehao Yu, Torsten Sattler, and Andreas Geiger. Gaussian Opacity Fields: Efficient and compact surface reconstruction in unbounded scenes. *arXiv preprint arXiv:2404.10772*, 2024.
- [69] Jingyang Zhang, Yao Yao, Shiwei Li, Tian Fang, David McKinnon, Yanghai Tsin, and Long Quan. Critical regularizations for neural surface reconstruction in the wild. In *Proceedings of the IEEE/CVF Conference on Computer Vision and Pattern Recognition*, pages 6270–6279, 2022.
- [70] Wenyuan Zhang, Kanle Shi, Yu-Shen Liu, and Zhizhong Han. Learning unsigned distance functions from multi-view images with volume rendering priors. *European Conference on Computer Vision*, 2024.

- [71] Wenyuan Zhang, Ruofan Xing, Yunfan Zeng, Yu-Shen Liu, Kanle Shi, and Zhizhong Han. Fast learning radiance fields by shooting much fewer rays. *IEEE Transactions on Image Processing*, 32:2703–2718, 2023.
- [72] Junsheng Zhou, Yu-Shen Liu, and Zhizhong Han. Zero-shot scene reconstruction from single images with deep prior assembly. In *Advances in Neural Information Processing Systems*, 2024.
- [73] Junsheng Zhou, Baorui Ma, Shujuan Li, Yu-Shen Liu, and Zhizhong Han. Learning a more continuous zero level set in unsigned distance fields through level set projection. In *Proceedings of the IEEE/CVF international conference on computer vision*, 2023.
- [74] Junsheng Zhou, Baorui Ma, Yu-Shen Liu, Yi Fang, and Zhizhong Han. Learning consistency-aware unsigned distance functions progressively from raw point clouds. In *Advances in Neural Information Processing Systems*, 2022.
- [75] Junsheng Zhou, Baorui Ma, Yu-Shen Liu, and Zhizhong Han. Fast learning of signed distance functions from noisy point clouds via noise to noise mapping. *IEEE Transactions on Pattern Analysis and Machine Intelligence*, 2024.
- [76] Junsheng Zhou, Baorui Ma, Wenyuan Zhang, Yi Fang, Yu-Shen Liu, and Zhizhong Han. Differentiable registration of images and lidar point clouds with voxelpoint-to-pixel matching. *Advances in Neural Information Processing Systems*, 36, 2024.
- [77] Junsheng Zhou, Weiqi Zhang, and Yu-Shen Liu. DiffGS: Functional gaussian splatting diffusion. In *Advances in Neural Information Processing Systems*, 2024.
- [78] Zihan Zhu, Songyou Peng, Viktor Larsson, Zhaopeng Cui, Martin R Oswald, Andreas Geiger, and Marc Pollefeys. Nicer-SLAM: Neural implicit scene encoding for rgb slam. In *2024 International Conference on 3D Vision (3DV)*, pages 42–52. IEEE, 2024.

A Appendix

A.1 Background Reconstruction



Figure 8: Visualization of reconstructed backgrounds.

Since our SDF field was learned by fitting Gaussian ellipsoids, it can infer implicit surfaces at any location where Gaussians are distributed. Therefore, our method has the same capability to reconstruct backgrounds as methods like TSDF fusion, as shown in Fig. 8. Current works generally utilize screened Poisson or TSDF fusion to reconstruct meshes [25, 20] and tend to reconstruct large sky spheres in the background. Our method learns neural SDFs and utilize marching cubes to reconstruct mesh, which avoid such bad cases.

A.2 Theoretical Analysis

We provide a theoretical analysis here to demonstrate the advantage of pulling queries onto disks compared to pulling queries onto centers. We provide a visual comparison of the two strategies in Fig. 9, showcasing the changes of the loss function and the loss gradients as the query point approaches the Gaussian center. As the query point gets closer to the Gaussian center, the loss function of “pulling to centers” decays at a constant rate, and the gradient of the loss remains constant. In contrast, for “pulling to disks”, the loss function decreases quadratically, and the gradient of the loss gradually diminishes. This means that under the influence of the disk loss, as the query point approximates the center, the received gradient becomes smaller, reducing the driving force that pushes the query point towards the center. In other words, the disk loss has a higher “tolerance” for the query point not being pulled to the center. This explains why we can learn a continuous field from a sparse and non-uniformly distribution of Gaussian ellipsoids using the disk loss, whereas the center loss would lead to the SDF field overfitting to every Gaussian center.

A.3 Limitations & Future Works

While our method successfully recovers accurate appearance and geometry reconstruction for a wide range of objects and scenes, it also has several limitations. Firstly, the neural SDF is seamlessly integrated with Gaussian ellipsoids, making it difficult to avoid the inherent drawbacks of original 3D Gaussians, such as the lack of transparent objects and areas with strong specular reflections. Secondly, although we address the issue of learning a continuous SDF field from sparse and non-uniformly distributed Gaussian ellipsoids by pulling query points to disks,

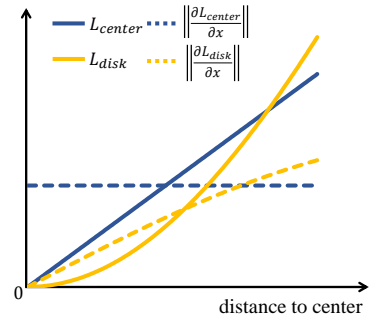


Figure 9: Visualization of loss and gradient between *Pulling to centers* and *Pulling to disks* with the distance of a query point to the Gaussian center.

the SDF field overfitting to every Gaussian center.

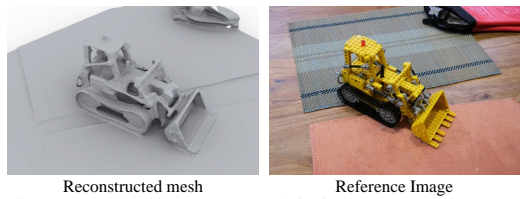


Figure 10: Failure case. This is because the SDF network cannot accurately capture high-frequency details due to the smooth characteristic of MLPs.

our method shows limited performance in extremely sparse areas. In very distant regions of unbounded scenes or areas with colors similar to the background color, where 3DGS reconstructs no ellipsoids or only a few ellipsoids, our method tends to produce holes. Thirdly, due to the continuous and smooth characteristics of MLPs, our SDF tends to capture the low-frequency features of objects, making it difficult to reconstruct high-frequency details. A failure case is shown in Figure 10, where we can reconstruct the very smooth tablecloth but fail to recover the details of the lego. There are two potential solutions for this issue in the future: one is to enhance the representation capability of the SDF by integrated with latest implicit representation learning methods, such as BACON [41] and GridPull [7]; the other one is to dig into the capabilities of TSDF fusion and screened Poisson in reconstructing our SDF field, which have the ability to reconstruct arbitrary resolution details.

A.4 More Results

We provide additional reconstruction results in Fig. 11, 12, 13, which further justifies the superiority of our method. We notice that there are some holes on the flowerbed area in Fig. 13. This is due to the overly complex geometric structures and a lack of view covering, thus emitting a significant under-fitting issue. This results in a set of extremely sparse, huge, and unevenly distributed Gaussians, which makes Gaussians are thick ellipsoid like shape rather than relatively thin plans, leading to poor sense of surface. Although these huge Gaussians may work well in rendering, but they cannot recover any geometry covered by them. How to control the size of Gaussians for SDF inference could be an interesting future work direction.

We also visualize the error maps on meshes obtained by 2DGS and ours in Fig. 14, which highlights our superiority in terms of the accuracy of extracted surfaces. The surfaces learned by 2DGS are usually fat and a little bit drift away from ground truth surfaces, although their meshes seem to show more details. Our method is able to capture more accurate surfaces by using 3D Gaussians pulled onto the zero-level set and pulling query points onto Gaussian disks at the same time, leading to much more accurate zero-level set.



Figure 11: More visualization results on DTU dataset.



Figure 12: More visualization results on TNT dataset.



Figure 13: More visualization results on MipNeRF 360 dataset.

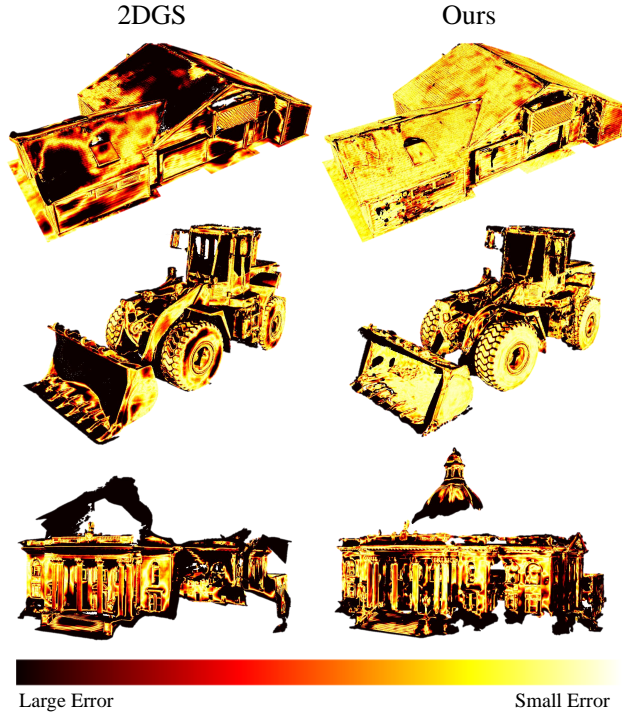


Figure 14: Error maps between 2DGS and our method on TNT dataset.

A.5 Discussion

About open surfaces. Since there are lots of non-closed surfaces in large-scale scenes, a natural solution is to learn an unsigned distance field to reconstruct open structures [70, 73, 33]. However, extracting the zero-level set from UDF as a mesh surface is still a challenge, resulting in artifacts and outliers on the reconstructed meshes. We report the result of learning UDFs instead SDFs in Fig. 15, which shows the shortcomings of UDF learning. To avoid the influence of double-layer surfaces on evaluation accuracy under the SDF settings, we practically delete the back faces according to the visibility of each face under each camera view. Through this way, we can accurately reconstruct open structures with single-layer surfaces.

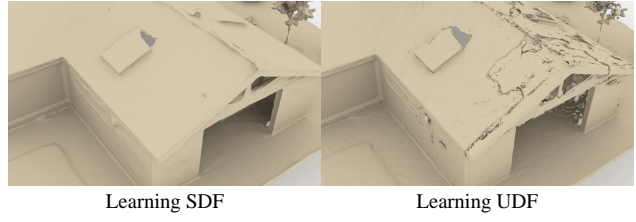


Figure 15: Visualization of surfaces reconstructed by SDF and UDF.